

Dynamical Model for Power Grid Frequency Fluctuations: Application to Islands With High Penetration of Wind Generation

María Martínez-Barbeito , Damià Gomila , and Pere Colet 

Abstract—We study the effects of a high share of wind generation on the frequency fluctuations of power grids on islands. We propose a dynamical model that includes conventional and variable renewable generation, as well as demand variations. Our model can assimilate load and generation data and reproduce frequency fluctuations with the current power mix with a high degree of accuracy, and it allows to simulate the frequency dynamics for different scenarios with a very high penetration of renewable energy. As a case study, we analyze the power grid of Gran Canaria island. We characterize the frequency fluctuations and propose a method to estimate the control needed to keep frequency deviations within reasonable limits.

Index Terms—Power grid, dynamical modelling, frequency fluctuations, frequency control, high renewable penetration, wind variability.

I. INTRODUCTION

THE need to mitigate climate change and decrease the dependency of the energy sector on hydrocarbons is accelerating the transition towards renewable energies. This transition relies on the electrification of the industrial, commercial, and domestic sectors. The International Energy Agency predicts an increase of 45% in electricity demand from 2015 to 2040 to be covered mainly by wind and solar power [1].

The energy transition is particularly pressing on islands, whose energy supply typically depends very much on imported fossil fuels and submarine connections to the mainland or nearby islands, which increases generation costs [2]. Although they only account for a small fraction of global greenhouse gas emissions, they are one of the most vulnerable territories to the effects of climate change. Nevertheless, typically there are abundant Variable

Renewable Energy Sources (VRES) present in islands. However, being small and with limited interconnectivity, islands' power grids are less robust than the mainland and they are subject to high demand variations and more frequent failures. The integration of a high share of VRES in islands' power systems highlights some of the grid stability challenges which are also present in larger systems [3], [4]. For these reasons, several authors have studied electricity generation and the integration of renewable energies in islands [5], [6], [7], [8], [9].

Stable power grid operation is based on the permanent balance between supply and demand, which keeps the grid at a reference frequency. Nowadays, due to the lack of large-scale storage capacity, electric power is generated in real-time to meet consumer needs. This is achieved given the dispatchable, i.e., controllable, nature of conventional energy sources. Besides, the inertia of conventional generators efficiently reduces the size of the frequency deviations. On the contrary, VRES are largely unpredictable and intermittent. Solar and wind power introduce power fluctuations at different timescales, adding difficulties to balance demand and production [10], [11]. Furthermore, they do not contribute to the global inertia of the grid, which directly affects its stability and operation, especially during low load hours [12], [13]. The problem of low inertia and how to overcome it by increasing the control capacity with different types of storage technologies has been addressed in the literature [14], [15], [16], [17], [18].

The progressive substitution of conventional power plants by VRES will reduce both the inertia of the system and the frequency control capabilities, decreasing the overall flexibility of the grid [19], [20]. Thus, higher reserve requirements and additional control strategies based on other technologies, such as batteries or other forms of storage and demand-side management, will be needed to eliminate undesirable power quality issues [21] and ensure the stable operation of the electric energy system. Therefore, several changes have to be made to integrate a high share of renewable generation. The most important being an increase in the amount of control, on the generation and/or the demand side [22], [23].

In this work, we address this issue by proposing a dynamical model for the high-voltage power grid. It includes conventional generators with primary and secondary frequency control and operation set point, VRES data assimilation, including its variability, demand data assimilation, and synthetic fast demand fluctuations. First, the model is calibrated on the basis of actual

Manuscript received 5 August 2022; revised 15 November 2022; accepted 18 December 2022. Date of publication 11 January 2023; date of current version 21 June 2023. This work was supported in part by the European Commission Innovation and Networks Executive Agency through the integrated action Virtual Power Plants for Islands, VPP4ISLANDS under Grant 957852, in part by MCIN/AEI/10.13039/501100011033/ and EU through FEDER funds under Grants PACSS RTI2018-093732-B-C22 and APASOS PID2021-122256NB-C22, and in part by MCIN/AEI/10.13039/501100011033/ through Maria de Maeztu program under Grant MDM-2017-0711. Paper no. TSTE-00798-2022. (Corresponding author: María Martínez-Barbeito.)

The authors are with the Instituto de Física Interdisciplinar y Sistemas Complejos, IFISC (UIB-CSIC), Campus Universitat de les Illes Balears, 07122 Palma de Mallorca, Spain (e-mail: maria@ifisc.uib-csic.es; damia@ifisc.uib-csic.es; pere@ifisc.uib-csic.es).

Color versions of one or more figures in this article are available at <https://doi.org/10.1109/TSTE.2022.3231975>.

Digital Object Identifier 10.1109/TSTE.2022.3231975

measurements for Gran Canaria island, which we take as a case study. Due to its geographical location, wind is a major natural resource having provided 14% of the electric demand in 2019 [24]. Second, we analyze the frequency fluctuations in scenarios with increasing installed wind power. Finally, we determine the amount of additional control that would be needed to keep fluctuations in range in these scenarios and examine changes in the stress of the lines.

II. MODEL

Our model consists of a network of nodes interconnected via power transmission lines or links. We describe nodes as oscillators that interact and should be synchronized to the same frequency [25], [26], yet we distinguish two groups: conventional generators and consumers. Consumer nodes correspond geographically to substations, and they include the load attached to the substation.

Conventional generators are described by the well-known swing equation, which accounts for their inertial response. We consider a reference frame rotating at the power grid reference frequency f_R , with $\omega_R = 2\pi f_R$ being the reference angular frequency. The voltage phase angle θ_i and the angular frequency $\omega_i = 2\pi f_i$ of node i follow [27] (see Appendix):

$$\dot{\theta}_i = \omega_i \quad (1)$$

$$\dot{\omega}_i = \frac{\omega_R^2}{2\hat{H}_i(\omega_i + \omega_R)} (P_i^m - P_i^e), \quad (2)$$

where $\hat{H}_i = H_i P_i^G$, and H_i and P_i^G are inertia per unit power and nominal power generation of node i . Equations (1) and (2) relate θ_i and ω_i with the supplied mechanical power P_i^m and the electric power P_i^e at the node. The latter will be discussed later.

At difference with Kuramoto-like models [28], [29], we include power plant frequency control loops to guarantee normal operation upon changes in the load. Primary control acts within a few seconds to stop the frequency drift by adjusting the speed governor. Then, secondary control takes over and activates spinning reserve power to restore the frequency back to its nominal value within a few minutes [27]. Primary and secondary control dynamics are respectively described by:

$$\dot{P}_i^m = \frac{1}{\tau_i} \left[P_i^s - P_i^m - \frac{P_i^c}{R_i} \frac{\omega_i}{\omega_R} \right] \quad (3)$$

$$\dot{P}_i^s = -\kappa_i \frac{\omega_i}{\omega_R}, \quad (4)$$

where τ_i is the turbine time constant, P_i^s the spinning reserve power, R_i the governor speed regulation parameter, P_i^c the primary control power, and κ_i the secondary control gain parameter.

For a single power plant, the secondary control adjusts the generation to cover the demand. For grids with several plants, the model as written so far adjusts the total generation to cover the demand, but the fraction of the generation provided by each plant is not determined. This is not the case of actual power systems, in which the distribution of the generation is planned beforehand by the grid operator. To this aim we break the indeterminacy by

adding a term in (4), which forces the plant to operate close to a given set point P_i^{ref} , i.e.,

$$\dot{P}_i^s = -\kappa_i \frac{\omega_i}{\omega_R} - \frac{1}{\tau_i^{\text{ref}}} (P_i^s - P_i^{\text{ref}}), \quad (5)$$

where τ_i^{ref} is the timescale of the forcing. This allows the assimilation of actual generation dispatch data into the model while plants still have primary and secondary control capabilities to compensate for supply-demand imbalances. In particular, we can force plants to operate close to zero generation by setting $P^{\text{ref}} = 0$. In this case, the power output is negligible, but the plant still contributes to the global inertia and control capacity of the system. To fully switch off a plant, we also set $P_i^c/R_i = 0$, $\kappa_i = 0$, and \hat{H}_i to be that of a consumer node (see next paragraph).

Consumer nodes, aside from the obvious lack of generation, do not have, in principle, mechanisms of frequency control. Nevertheless, they still have some residual inertia arising, for instance, from electric motors. Thus, we model them using (1), (2) with a very small value of \hat{H}_i as compared to that of power plants, and $P_i^m = 0$.

VRES are characterized by their intermittent and unpredictable nature, which makes renewable generation quite different from conventional plants. Regarding the inertial response, VRES have little to offer: solar units are inertialess, and wind turbines store some kinetic energy but it is not inherently available. Nonetheless, some frequency control mechanisms can be implemented effectively through the AC converter power electronics [12]. For simplicity, we model VRES generation as a frequency-independent negative demand. VRES energy fed into the network is taken from actual data provided by the system operator.

Finally, for any node the electric power P_i^e is given by

$$P_i^e = \left(1 + D_i \frac{\omega_i}{\omega_R}\right) P_i^l + \sum_j B_{ij} \sin(\theta_i - \theta_j) - P_i^{\text{VR}}. \quad (6)$$

The first term in (6) accounts for the load in node i , P_i^l , including a frequency-sensitive load fraction D_i which introduces damping. The second term describes the power transmission from node i to other nodes j within the lossless line approximation. Transmission lines are characterized by the susceptance parameter $B_{ij} = V_{ij}^2/Z_{ij}$, set by the line voltage V_{ij} and impedance Z_{ij} . The last term corresponds to the energy generated from VRES sources associated to node i , if any.

This model is highly versatile and can be used to efficiently simulate the dynamics over periods of months, allowing to explore different scenarios towards fully renewable power grids. The Fortran source code for the model has been uploaded to a repository [30]. Grids can be of any size and include any generation technologies provided enough inertia is always present in the system so that it is not necessary to account for sub-second timescale dynamics [31]. Inertia can come from conventional power plants or converters capable of inertia emulation on the generation side, and from synchronous electrical motors on the demand side. In fact, it can be argued that even a 100% renewable power grid will not have vanishing inertia [32]. In cases of

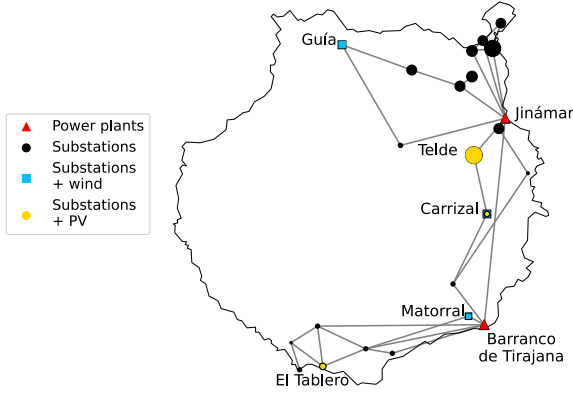


Fig. 1. Gran Canaria high-voltage power grid. Node size proportional to load.

TABLE I
CONVENTIONAL POWER (MW) INSTALLED IN GRAN CANARIA. SOURCE:
MONITOR DELOITTE [36]

	<i>B. de Tirajana</i>	<i>Jinámar</i>
CCGT	433.1	—
Steam turbine	148.4	111.2
Gas turbine	64.6	82.2
Diesel engine	—	41.0
Total	646.1	234.4

extremely low inertia, electromagnetic transients at timescales beyond those considered here must be taken into account [19], [31], [32], [33].

A. Gran Canaria Grid

We analyze the case of Gran Canaria, within the Spanish Canary Islands archipelago in the Atlantic Ocean. Its high-voltage grid can be mapped down to substation level as the network of 23 nodes and 33 links shown in Fig. 1 [24]. Not being connected to mainland, electricity is mainly generated at two facilities: Barranco de Tirajana and Jinámar. Each facility includes groups with different conventional generation technologies, such as combined cycle gas turbines (CCGT), steam turbines, gas turbines, and diesel engines (see Table I). For the model, we consider each technology at each facility as an individual plant, thus a total of 6 power plants are included. Plants at a given facility are connected through short large-capacity lines to a node with zero load, which is connected via regular transmission lines to the rest of the grid.

Besides conventional plants, there is also wind generation and, to a less extent, photovoltaic (PV) generation. For reference, the total consumption in 2019 was 3581.9 GWh, where 498.4 GWh (13.9%) was covered by wind and 55.4 GWh (1.5%) by PV generation. Wind is clearly a major natural resource owing to trade winds that blow all year round. Wind turbines are mainly located in the southeast, which we consider as connected to the nodes of Matorral and Carrizal. There are also wind turbines in the northwest, which we consider connected to the node of Guía.

PV generation is connected to the nodes of Telde, Carrizal, and El Tablero.

Finally, the voltage of the transmission lines can be found in [24]. We estimate the impedance of the lines from their length as in [34]. The length of the lines has been measured approximately from maps.

B. Demand Data and Demand Model

The Spanish grid operator, Red Eléctrica España (REE), provides aggregated generation and demand data for Gran Canaria with a time granularity of 10 minutes [35]. We distribute the total demand among the nodes proportionally to their population and interpolate between consecutive data points to avoid artificial jumps.

Actual demand has fluctuations at faster timescales which can be modelled as a result of many devices switching on and off randomly [25]. The resulting power spectrum for the demand is similar to that of an Ornstein-Uhlenbeck stochastic process. Here, we model the demand as

$$P_i^1(t) = \tilde{P}_i^1(t) (1 + \epsilon_{ou} \xi_i^{ou}(t)), \quad (7)$$

where \tilde{P}_i^1 is the interpolated demand of node i , ϵ_{ou} the noise amplitude, and ξ_i^{ou} are Ornstein-Uhlenbeck processes with zero mean and correlation $\langle \xi_i^{ou}(t) \xi_j^{ou}(t') \rangle = \delta_{ij} \frac{1}{2\tau_{ou}} e^{-|t-t'|/\tau_{ou}}$, where τ_{ou} is the correlation time.

C. Generation Data

REE disaggregates conventional generation data by technology. For each technology, we distribute the scheduled generation proportionally to the plants' nominal capacity (see Table I) to set P_i^{ref} . Unlike the demand, P_i^{ref} is a step-like quantity resembling a dispatch made for 10-minute intervals.

REE 10-minute data also includes wind and PV generation. Wind generation is interpolated and distributed evenly among the three nodes to which it is connected. Similarly for PV generation.

D. Parameter Values

The model has several parameters that need to be determined. Some of them are well known, such as the reference frequency f_R . For others, nominal values can be found in the literature: H ranges from 1 to 10 s depending on the machine size and type [27]; D is usually taken between 0 and 2 [37]; τ is in the range of 0.2 to 2.0 s [27]; and R is typically around 5 or 6 percent [27], [37].

The remaining parameters were fitted by comparing simulated frequency and power plant generation to available data:

- ϵ_{ou} and P^c have an opposite effect. Increasing the noise amplitude requires increasing primary control in order to keep constant the amplitude of frequency fluctuations. We have chosen these parameters so that the amplitude of the fast deviations of the simulated frequency matches that of the data. We have seen that a good choice is taking P^c around 10% of the installed power for each generation group, except for gas turbines, which is 20%; while ϵ_{ou} is

TABLE II
PARAMETER VALUES FOR THE REFERENCE CASE

Power plant parameters							
Barranco de Tirajana				Jinámar			
	CCGT	Steam t.	Gas t.	Diesel	Steam t.	Gas t.	
H	4.5	3.0	5.5	2.0	3.0	5.5	s
P^c	45.0	15.0	12.0	4.0	10.0	16.0	MW
κ	7.0	1.5	1.2	0.4	1.0	1.6	MW/s
τ^{ref}	60	30	30	30	30	30	min

Common parameters			Noise parameters		
f_R	50	Hz	τ_{ou}	60	s
D	1	-	ϵ_{ou}	0.15	-
τ	0.5	s			
R	0.05	-			
$\hat{H}_{\text{consumers}}$	10^{-4}	MWs			

such that the amplitude of fast demand variations is within a reasonable range.

- b) τ^{ref} and κ are also interrelated. Decreasing τ^{ref} increases the forcing towards P^{ref} , reducing the capability to change generation according to frequency deviations. Increasing κ has the opposite effect. However, there are situations in which the two forcing terms for P^s have the same sign. For instance, under a sustained demand increase $\omega < 0$ while the grid operator sets P^{ref} larger than the current generation, thus both forcing terms cooperatively increase P^s . In Section II-E, we discuss an analytical approximation to determine the total control capability. We distribute this total control among the plants proportionally to P_i^c but taking into account that the CCGT power plant, being the most advanced technology, has a larger control capability. Then, we have taken $\tau^{\text{ref}} = 30$ minutes for each generation group (60 minutes for CCGT) during normal operation and 10 minutes when they are switched on or off.
- c) Finally, for τ_{ou} , we have chosen 60 seconds because it is a reasonable value for the correlation between changes in the demand. This assumption is supported by the power spectrum as discussed in Section III.

Following this procedure, we determine the set of parameter values listed in Table II, which we consider for the reference case and the base for future scenarios.

E. Analytical Estimation of the Secondary Control Gain

In order to estimate the secondary control, we start by deriving an approximation for the global secondary control gain $\kappa = \sum_i \kappa_i$ as follows. Secondary control acts in response to frequency deviations caused by supply-demand imbalances bringing ω to zero. It does this at a timescale set by κ , typically a few minutes. If a supply-demand imbalance is sustained over time, the secondary control keeps adjusting P^s in an attempt to bring ω to zero. For a sustained linear increase in demand, simulations show that, after a transient, the generation ramp induced by the secondary control matches exactly the demand ramp (see Fig. 2(a)). Thus, the frequency gets a constant offset f_0 . Assuming a single power plant, no VRES generation and constant $\omega = \omega_0 = 2\pi f_0$, from (2) and (6), we have

$$P^{\text{m}} = (1 + D\omega_0/\omega_R)P^{\text{l}}, \quad (8)$$

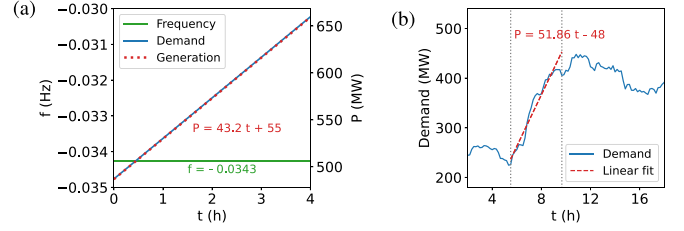


Fig. 2. (a) Response of the model of a single power plant to a sustained linear demand increase. (b) 10-minute demand data.

where $P^{\text{l}} = \sum_i P_i^{\text{l}}$. Integrating (4), we have

$$P^s = P_0^s - \kappa t \omega_0 / \omega_R. \quad (9)$$

Introducing (8) and (9) in (3), and isolating ω_0 / ω_R , we have

$$\frac{\omega_0}{\omega_R} = \frac{P_0^s - \tau \dot{P}^{\text{l}} - P^{\text{l}}}{\tau D \dot{P}^{\text{l}} + \kappa t + D P^{\text{l}} + P^c / R}. \quad (10)$$

Taking $P^{\text{l}} = a_1 + b_1 t$, in the limit of large times, we have

$$\kappa = -b_1 \left(D + \frac{\omega_R}{\omega_0} \right) \approx -b_1 \frac{\omega_R}{\omega_0}. \quad (11)$$

To estimate κ , we consider a period of time with a sustained increase in the demand, as the one of four hours delimited by vertical dashed lines in Fig. 2(b), and perform a linear fit to determine $b_1 = 51.86 \text{ MW/h} = 0.0144 \text{ MW/s}$. We are interested in the frequency offset triggered by the ramp. To smooth the fast frequency fluctuations, we average the frequency over the period considered. We determine an offset $f_0 = -0.035 \text{ Hz}$, and from (11), we get $\kappa = 20.6 \text{ MW/s}$.

However, this estimation of κ neglects dispatch operations. The system operator sets the operating points of power plants according to the predicted demand profile. In particular when demand is expected to grow, P^{ref} is set to a larger value contributing with the secondary control to drive P^s up. Thus, the above calculation overestimates the value for κ . The final value $\kappa = 12.7 \text{ MW/s}$ has been obtained by matching simulation results to data.

Other methods have been proposed to estimate the amount of control in a power system from the time series of frequency fluctuations. In [38], for instance, the authors propose a procedure based on considering an aggregated swing equation to model the power grid and determine the most likely values for the control parameters. In our case, this procedure cannot be straightforwardly applied as, on one hand, we describe the primary and secondary response by separate equations, and on the other, we use coloured noise instead of white, hindering the relationship between the parameters of the two models.

III. MODEL VALIDATION

We now validate the model by running simulations for different parameter values and comparing the results with frequency measurements collected in the Power Grid Frequency Database [39], [40]. This database has data for Gran Canaria for two periods, February 4 to 10, 2018, and November 25 to 26, 2018, at a sample rate of 1 s. The initial and final days of each

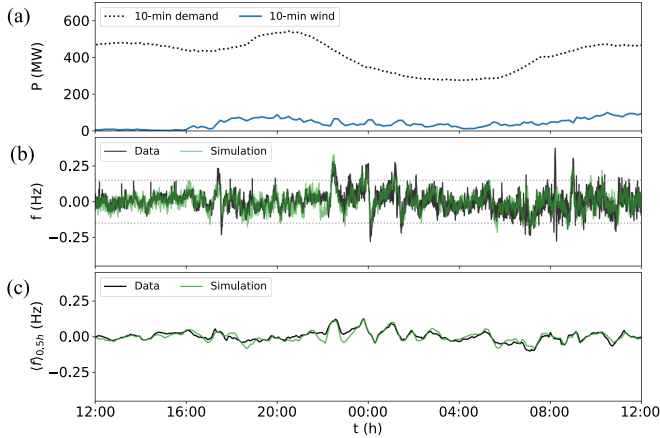


Fig. 3. Evolution of (a) demand (dotted black line) and wind generation (solid blue line) in Gran Canaria from 12:00 07-02-2018 to 12:00 08-02-2018; (b) frequency fluctuations given by the model (green line) in comparison to measured data (black line); and (c) rolling average of frequency deviations using a 30-minute window. The dotted line at ± 0.15 Hz in (b) indicates the statutory limits [41].

period are not complete, thus we consider February 5 to 9, 2018 to calibrate the model.

Fig. 3(a) shows the total demand and the total wind generation obtained from REE [35] for 24 hours. Panel (b) shows the frequency-time trace predicted by the model (green line) using the parameter values given in Table II on top of the measured data (black line). Both time series show larger frequency fluctuations the larger the wind generation ratio and its variability are. This is because, besides demand fluctuations, renewable generation adds a new source of variability, but this time on the generation side.

In general, from Fig. 3, we see that the model correctly captures frequency deviations in accordance to wind power ramps. However, there are some discrepancies between data and simulation results, which might be due to two different factors. Since we do not have precise information on which generation groups are working at each moment, nor on their control capabilities, we set primary and secondary control parameters constant throughout the day. But, in the actual system, the amount of control changes depending on the amount and type of generators operative. Thus, we might over or underestimate the control in certain periods of the day.

Moreover, we feed the model with 10-minute data, which misses information on changes at faster timescales. We use an Ornstein-Uhlenbeck process to model small random changes in demand at fast timescales. However, this will not reproduce large events occurring at timescales below 10 minutes, such as wind gusts, sudden large changes in consumption, or contingencies in generation. We think this is the reason behind peaks in the frequency data not reproduced by the simulation, as the one observed around 8:00 (Fig. 3).

Nevertheless, the model reproduces frequency data with reasonable accuracy as further indicated by the rolling average over a 30-minute sliding window shown in Fig. 3(c). The correlation coefficient between the empirical and the simulation time series is $r = 0.82$.

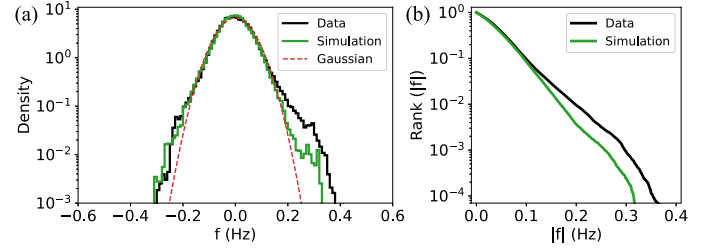


Fig. 4. (a) Probability density and (b) rank-size distribution of frequency fluctuations from 05-02-2018 to 09-02-2018.

TABLE III
COMPARISON BETWEEN THE MOMENTS OF THE PROBABILITY DENSITY OF MEASURED AND SIMULATED FREQUENCY FLUCTUATIONS

Moment	Data	Simulation
Mean	50.00 Hz	50.00 Hz
Standard deviation	0.06 Hz	0.06 Hz
Skewness	0.42	0.02
Kurtosis	4.95	4.15

We now consider the statistical properties measured over the whole validation period. In Fig. 4(a), we compare the probability density of the measured frequency fluctuations (black line) with that from simulations (green line). For comparison, the red dashed line corresponds to a Gaussian distribution. The mean, standard deviation, skewness, and kurtosis are given in Table III. Empirical and simulation distributions are quite similar, with a mean of 50 Hz, a standard deviation of 0.06 Hz, and a kurtosis over 4. Since the kurtosis of Gaussian distributions is 3, empirical and simulated frequency distributions are clearly leptokurtic, which means that the probability of large events is larger than for the Gaussian [42]. This is in line with the findings reported in [43], where different grids were analyzed and their frequency fluctuations were better described by Lévy-stable and q-Gaussian distributions instead.

The main disagreement between empirical and simulation statistics is found in the skewness. The empirical distribution is more skewed to the right than that obtained from the simulation, which is almost symmetric. Note that the two distributions agree very well for negative frequency fluctuations. The disagreement on the right tail could be motivated by large wind gusts or sudden demand drops occurring at timescales faster than 10 minutes, not collected in wind or demand data, and which would trigger a large positive frequency deviation that cannot be reproduced by the model.

We also compute the complementary cumulative distribution of the absolute frequency deviations $|f|$ from the time series as follows. We reorder the data from the smallest to the largest, and evaluate the rank of the frequency deviations as $R(|f_k|) = 1 - (k - 1)/(N - 1)$, where N is the number of data points. Then, $R(|f|)$ measures the probability to have a frequency fluctuation of size larger than $|f|$. Results are plotted in Fig. 4(b), where we observe that the model fits well for small deviations but it is not as good to predict the probability of the largest ones. This disagreement comes from the differences in the right tail of the frequency distribution discussed above.

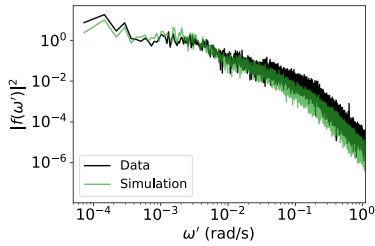


Fig. 5. Power spectrum of the frequency fluctuations from 05-02-2018 to 09-02-2018. ω' are the Fourier sample frequencies, not to be confused with the angular frequency ω in the model.

Finally, in Fig. 5, we also calculate the power spectrum of the frequency fluctuations. We observe an excellent agreement for timescales slower than 5 minutes ($\omega' < 0.02$ rad/s). For faster timescales (large ω'), the dynamics is dominated by the fast fluctuations, and the power spectrum obtained from the simulation with synthetic noise deviates slightly from the empirical one.

IV. RESULTS AND DISCUSSION

A. Scenarios With Large Penetration of Wind Generation

In this section, we simulate scenarios with a large penetration of renewable energies by analyzing the effects of increasing the installed wind power capacity on frequency fluctuations.

We take 2019 as the reference case, when the installed wind power in Gran Canaria was 159.33 MW according to the Instituto Canario de Estadística (ISTAC) [24]. We perform simulations for increasing amounts of wind capacity in the system while keeping demand and total generation unchanged as follows. We multiply the 2019 wind generation data by a scaling factor n , and we use the notation $W \times n$ to refer to the scenarios. At each dispatch time, to match the demand, we reduce conventional generation accordingly. This is done by keeping the same plants operative but decreasing P^{ref} plant by plant. We start reducing P^{ref} for the smallest plant operative at that time. If reducing the smallest plant's P^{ref} to zero is not sufficient, we reduce P^{ref} for the second smallest operative plant, and so on. Plants keep inertia and control capabilities even if P^{ref} is reduced to 0.

In Fig. 6, we show the evolution of the frequency for January 19, 2019, considering the reference wind generation ($W \times 1$, light blue), as well as scenarios with four ($W \times 4$, blue) and eight ($W \times 8$, dark blue) times this amount. The higher the wind penetration, the larger the wind fluctuations become, causing larger frequency deviations. For $W \times 1$, wind generation covers a small fraction of the demand, and frequency deviations stay close to the statutory limits of ± 0.15 Hz, as shown in panel (b). However, for $W \times 4$, wind becomes the main source of generation for most of the day, and the effect of wind variations is magnified. In turn, frequency deviations become larger, except for the time window where the wind generation exceeds the demand (around 16:00). In this case, we only feed into the grid the demanded amount. The excess power is simply discarded. Curtailment in the case of extra wind generation can be considered a mechanism of frequency control. This is a benefit of having some overcapacity for VRES [44]. For $W \times 8$, wind generation usually exceeds the

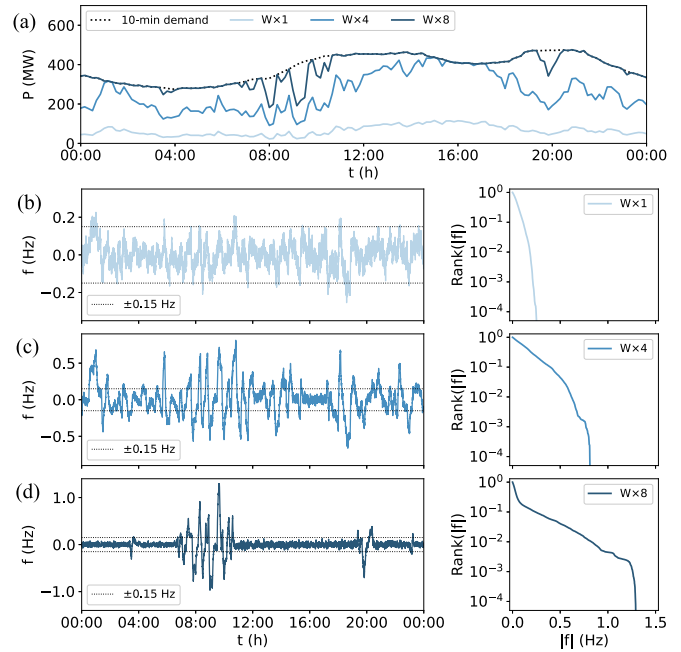


Fig. 6. Comparison of the frequency fluctuations for the current installed wind capacity ($W \times 1$) and two scenarios with 4 ($W \times 4$) and 8 ($W \times 8$) times the current capacity. (a) Demand and wind generation for 19-01-2019. (b)–(d) Frequency fluctuations given by the model for each scenario. The right column shows the rank of the frequency fluctuations. Model parameters given in Table II.

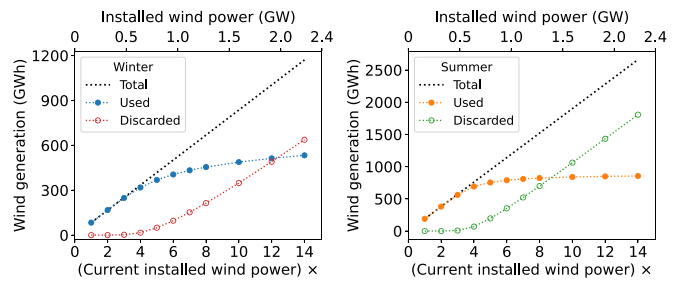


Fig. 7. Evolution of the used, discarded, and total wind generation during winter and summer as a function of the installed wind power. For comparison, the total demand was 857.5 GWh in winter and 902.15 GWh in summer.

total demand. Curtailment together with the inertia and control provided by operative plants (despite operating at $P^{\text{ref}} = 0$) allow maintaining the frequency close to the reference value. However, there are still intervals characterized by very strong wind variations (for instance, from 7:00 to 11:00), which lead to frequency deviations well beyond statutory limits.

We have analyzed the amount of curtailed energy in winter (20-12-2018 to 20-03-2019) and summer (20-06-2019 to 20-09-2019) periods separately. Trade winds are stronger during the summer, and weaker and more intermittent in winter. Demand is also larger in summer than in winter, associated with tourism and larger needs for air conditioning cooling. Fig. 7 shows the evolution of the used and discarded wind generation as wind capacity increases. Despite the difference in the amount of wind generation during winter and summer, we see a similar behavior in both cases. As expected, increasing the capacity from the current value leads to increasing generation, with practically no

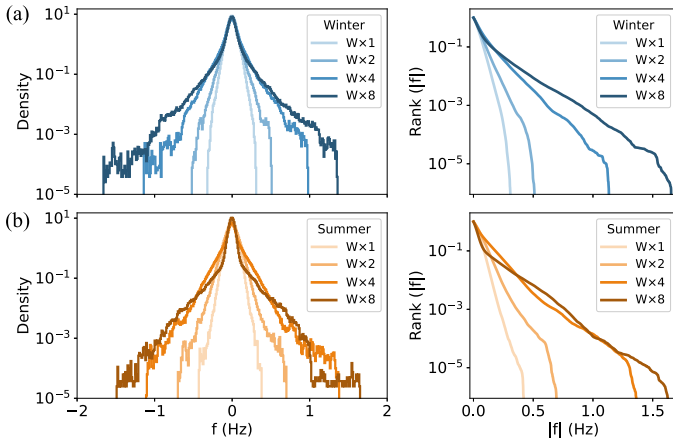


Fig. 8. Probability density (left) and rank-size distribution (right) of frequency fluctuations during (a) winter and (b) summer resulting from simulations. Color shades from lightest to darkest correspond to 2019 wind capacity ($W \times 1$), twice this capacity ($W \times 2$), four times ($W \times 4$) and eight times ($W \times 8$).

curtailment. At about $W \times 4$, any additional capacity cannot be fully utilized and curtailment starts. The curve of the used energy becomes sublinear and eventually reaches a plateau. In summer, for $W \times 8$, the amount of curtailed energy already exceeds the used one. In winter, the same happens above $W \times 12$. In fact, way before these crossovers, the used energy curve is quite flat, and we could conclude that increasing the installed capacity by a factor much beyond 5 would only make sense if curtailment was intended for control purposes.

Next, we analyze the changes in the frequency statistics. In Fig. 8, we show the probability density and the rank-size distribution of the frequency fluctuations obtained from simulations performed over the whole winter or summer period. Regarding the probability density, we observe that the distribution becomes broader as the amount of wind increases. But, at some point, the tails become longer and the peak narrows. The change in shape can be understood considering periods of large wind variability leading to long tails, together with periods where wind generation exceeds demand, in which curtailment reduces frequency fluctuations. As a result, the probability of large frequency deviations increases, while the probability of medium size deviations decreases. This effect can also be seen in the rank-size distribution as it changes from a parabolic to a more shoulder-like shape. Note, also, that for large wind capacity there are long periods of the day with very small fluctuations (see, for instance, Fig. 6(d) between 11:00 and 19:00), thus the probability of very small fluctuations increases.

Although for a given wind capacity frequency fluctuations are larger in summer than in winter, in practice, frequency fluctuations will be more severe in winter. The reason is that covering a given fraction of the demand with wind generation requires a larger wind capacity in winter than in summer. For instance, covering around 40% of the demand by wind generation requires in winter $W \times 4$, with fluctuations larger than 1 Hz, while in summer only $W \times 2$ is needed and fluctuations would stay within 0.7 Hz. Both cases are unacceptable for power grid operation.

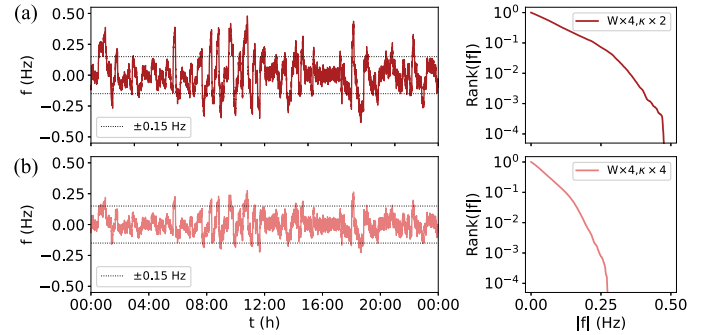


Fig. 9. Frequency fluctuations given by the model in two scenarios with 4 times the current wind capacity ($W \times 4$) and different amounts of secondary control. Model parameters, except κ , as in Table. For reproducibility: 19-01-2019.

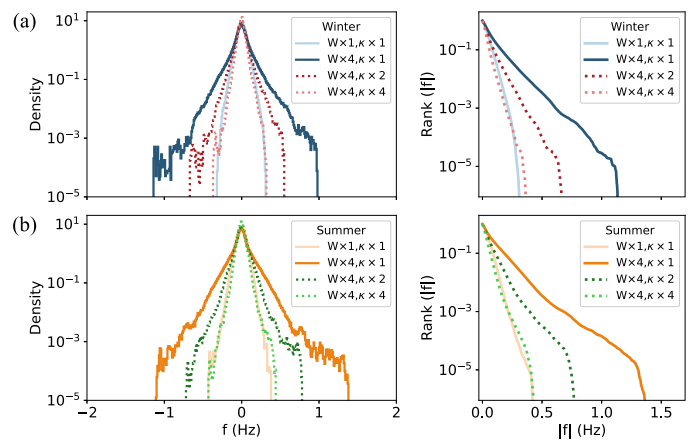


Fig. 10. Probability density function and rank-size distribution of frequency fluctuations in different scenarios.

In the next section, we study the extra control needed to keep the frequency within the statutory limits.

B. Estimation of Additional Control Needs

The main challenge to be solved in order to integrate a high share of renewable energies into the grid is to keep frequency fluctuations within reasonable limits. To do so, it is necessary to increase control. In our case, since we have demand and generation data every 10 minutes, we focus on secondary control, which is responsible for adjusting the frequency at the timescale of minutes.

In Fig. 9, we plot the frequency evolution predicted by the model for January 19, 2019, in scenarios with four times the reference wind capacity ($W \times 4$), and twice ($\kappa \times 2$) and four times ($\kappa \times 4$) the reference secondary control. Comparing these plots to Fig. 6(c), where we have $W \times 4$ and $\kappa \times 1$, we observe that increasing secondary control reduces the size of all frequency deviations.

In Fig. 10, we plot the probability density function (left) and rank-size distribution (right) of frequency fluctuations. We show, for the whole winter and summer periods, the reference case ($W \times 1, \kappa \times 1$) and scenarios with $W \times 4$ and: a) current control capability ($W \times 4, \kappa \times 1$), as in Fig. 8; b) twice ($W \times 4, \kappa \times 2$), and c) four times as much secondary control ($W \times 4, \kappa \times 4$). As

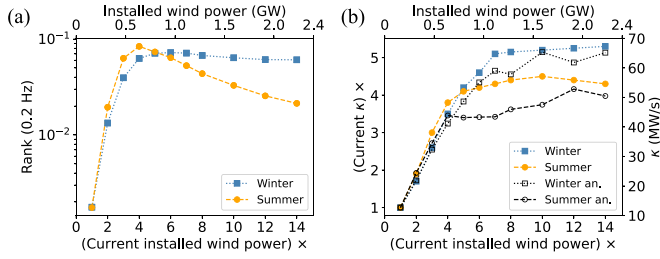


Fig. 11. (a) Probability of having fluctuations larger than 0.2 Hz as the installed wind power increases. (b) Secondary control needed in order to decrease fluctuations to the reference case.

we have seen for a single day, we observe that the seasonal distribution tends to that of the reference case as secondary control is increased.

In the remaining of this section, we address the question of how much control capacity is needed to stabilize the frequency in scenarios where wind provides a large fraction of the generated power. We do this using both numerical simulations and the analytical approach explained in Section II-E.

According to the Spanish legislation for non-peninsular power systems [41], frequency variations up to ± 0.15 Hz are considered normal, while deviations up to range ± 0.25 Hz can be accepted provided they last for less than 5 minutes. We take the intermediate value of 0.2 Hz and, in what follows, we consider a scenario acceptable when the probability of having absolute frequency deviations $|f|$ larger than 0.2 Hz, $R(|f| = 0.2)$, is equal or smaller than that with the reference wind capacity.

Fig. 11(a) shows $R(|f| = 0.2)$ for increasing wind capacity while keeping the reference control capacity. Initially, the probability of deviations larger than 0.2 Hz increases linearly with the wind capacity. However, it reaches a maximum at a specific point, which is smaller in summer than in winter, and then decreases. The decrease is more pronounced in summer. This is in agreement with the narrowing shape in the central part of the frequency density distribution for large wind capacity shown in Fig. 8. The reason is the effective control introduced by the curtailment of excess wind generation.

For each scenario, we increase the amount of control κ until $R(|f| = 0.2)$ is the same as in the reference case. Results are plotted with filled color markers in Fig. 11(b). As expected, the needed control increases linearly with wind capacity up to a point where curtailment starts to provide effective control, causing the need for additional control to reach a plateau.

For the analytical estimation of the control, we proceed as follows. We start by considering the reference case and, from (11), we estimate the load ramp b_l associated to a frequency offset $f_0 = 0.2$ Hz. Since $\kappa = 12.7$ MW/s, we have $|b_l| = 0.0508$ MW/s, which corresponds to an increment $|\Delta P^1| = 30.48$ MW in 10 minutes. Ramps larger than that would generate frequency deviations beyond 0.2 Hz. Next, we compute the net load provided by conventional plants by subtracting wind generation data from the 10-minute demand, construct the rank-size distribution of the differences between consecutive values $R_{\text{ref}}(|\Delta P^1|)$, and determine the probability to have a ramp larger than 30.48 MW

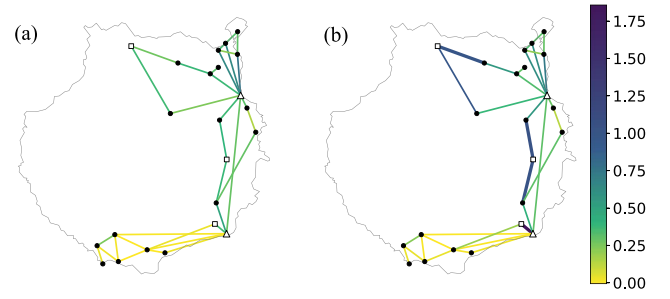


Fig. 12. 1-hour maximum line stress for: (a) the current wind capacity; and (b) 8 times this capacity. Markers distinguish the node type: Δ conventional power plants, \square substations with wind generation, and \bullet substations. In panel b) thick lines correspond to overloaded transmission lines (stress above 1).

in 10 minutes, namely $R_{\text{ref}}(|\Delta P^1| = 30.48)$, which turns out to be 5.5×10^{-4} in winter and 7.7×10^{-4} in summer.

Then, for scenarios with high wind penetration, we determine the net load provided by conventional plants, construct the rank-size distribution of the differences and determine the value of $|\Delta P^1|$ such that $R_{\text{scenario}}(|\Delta P^1|) = R_{\text{ref}}(30.48)$. With this value of $|\Delta P^1|$, we determine $|b_l|$. Finally, the value of κ is given by (11) with $f_0 = 0.2$ Hz.

We plot these results with empty black markers in Fig. 11(b). We see that the simulation results are similar to the analytical values for scenarios with up to $W \times 4$. However, for scenarios with a higher wind penetration, the analytical calculation underestimates the need for secondary control.

C. Transmission Lines

Transmission lines, designed to carry power over long distances with little losses, have a finite capacity. Here, we consider 70, 120, and 400 MVA for 66, 132, and 220 kV lines respectively. We define the stress of a line as the ratio between the power that flows through the line and its maximum transmission capacity.

In Fig. 12(a), we show in color code the maximum 1-hour average stress of each line during summer for $W \times 1$. We see that all lines always operate below their limits. However, the stress is larger in the northeast corner of the island, where the capital of Gran Canaria, Las Palmas, and the main consumption centers are located. We also see some lines operating at around half of their capacity. For instance, the lines connecting the two conventional power plants. This is because the biggest plant is actually the one in the south, which is the least loaded area. Therefore, a large fraction of the generated power must be carried to the north of the island.

Any change in the spatial load or generation distribution will alter the power flowing through the transmission lines of the network. Therefore, as we increase the installed wind power, the stress of the lines may change. In particular, the most susceptible lines are those connected to the three wind generation sites, as well as conventional generation facilities. The first due to an increase in the generation that replaces the latter.

In Fig. 12(b), we show the equivalent results for a scenario with $W \times 8$ and the reference control capability. Overall, an increase in the stress of the lines connecting the wind generation sites is clearly observed. In the south of the island, the

change in most of the lines is barely noticeable, i.e., they still operate at very low capacity. However, the short line connecting Matorral with Barranco de Tirajana (see Fig. 1) undergoes a major change. Its stress level highly increases and exceeds its maximum transmission capacity. This is because it is part of the shortest path to the north of the island, so it has to carry a lot of power. This line should clearly be upgraded if more wind power is connected to that node. In general, the stress level of the lines connected to the wind generation nodes increases. Besides, lines in the path from wind nodes to the largest consumption areas are also affected. We also note that there are lines with large stress variations depending on wind availability.

Finally, averaging the stress of all the lines in the grid, we find that the average stress grows with the installed wind power. We believe the issue is that the beneficial effect of redistributing the generation in more sites beyond the two conventional facilities is counteracted by the fact that the wind generation sites are further away from the main consumption centers. In order to reduce the stress levels of the lines, it would be necessary either to upgrade the current transmission lines or to install new ones.

V. CONCLUDING REMARKS

In this work, we have proposed a model for the high-voltage power grid, suitable to simulate the power grid frequency dynamics in scenarios of high penetration of VRES under realistic conditions and analyze the control needed to maintain frequency fluctuations within range. The model includes conventional generators with primary and secondary frequency control and operation set point, VRES and demand data assimilation, and fast synthetic demand fluctuations. We have validated the model against actual frequency measurements for the island of Gran Canaria. Despite the limitations in the available data, the model does a very good job of reproducing the actual frequency variability. More accurate results would be obtained if the demand and generation data had a finer temporal and spatial resolution.

Once the model has been validated, we have explored scenarios in which the wind capacity is increased while conventional generation is reduced. In these scenarios, frequency fluctuations typically exceed the statutory limits. For large wind capacity, curtailment of excess wind generation acts as an effective additional control. Nevertheless, there are periods of very large wind variability which translate into strong frequency deviations, even with the largest conventional plant providing inertia and control capabilities at all times.

We have determined the amount of additional secondary control in conventional plants necessary to keep frequency fluctuations within range. This has been done from numerical simulations and from an analytical approximation which turns out to work very well in scenarios without curtailment. The need for additional secondary control grows linearly with wind capacity up to a point in which it saturates due to the effective control provided by curtailment. We have also analyzed the changes in the stress of the lines when increasing wind capacity. We have found an overall increase in the line stress, mainly in the lines connected to the wind generation sites.

Finally, the model introduced here is quite flexible and can be adapted to the analysis of other scenarios, such as those associated to the increase of solar generation, the introduction of storage, or the use of demand control techniques. These analyses will be performed elsewhere.

APPENDIX

We derive the swing equation for a conventional generator following section 11.2 of [27]. From Newton's second law for rotation, the angular frequency of the rotator ω_m with respect to a fixed reference frame follows

$$J\dot{\omega}_m = T_m - T_e = (P_m - P_e)/\omega_m, \quad (12)$$

where J is the combined moment of inertia of the prime mover and the generator, T_m and T_e the mechanical and electromagnetic torque, and P_m and P_e the mechanical and electric power. We have used that power is torque times angular frequency. For a generator with p poles, the electrical angular frequency is $\omega_e = p\omega_m/2$, thus

$$\dot{\omega}_e = \frac{p^2}{4J\omega_e} (P_m - P_e). \quad (13)$$

Introducing the inertia per unit power $H = 2J\omega_R^2/p^2 P_G$ (ratio of the kinetic energy at the reference angular frequency ω_R to the rated power of the generator P_G) into (13), and defining $\omega \equiv \omega_e - \omega_R$ leads to (2).

REFERENCES

- [1] I. E. Agency, "World energy outlook 2020," 2022. [Online], Available: <https://www.iea.org/reports/world-energy-outlook-2022>
- [2] D. Weisser, "On the economics of electricity consumption in small island developing states: A role for renewable energy technologies?," *Energy Policy*, vol. 32, no. 1, pp. 127–140, 2004.
- [3] H. Bevrani, A. Ghosh, and G. Ledwich, "Renewable energy sources and frequency regulation: Survey and new perspectives," *IET Renewable Power Gener.*, vol. 4, no. 5, pp. 438–457, 2010.
- [4] R. Sims et al., "Integration of renewable energy into present and future energy systems," in *Proc. Special Rep. Renewable Energy Sources Climate Change Mitigation*, 2011, pp. 609–706.
- [5] Y. Kuang et al., "A review of renewable energy utilization in islands," *Renewable Sustain. Energy Rev.*, vol. 59, pp. 504–513, 2016.
- [6] G. Notton, "Importance of islands in renewable energy production and storage: The situation of the french islands," *Renewable Sustain. Energy Rev.*, vol. 47, pp. 260–269, 2015.
- [7] J. P. Praene, M. David, F. Sinama, D. Morau, and O. Marc, "Renewable energy: Progressing towards a net zero energy island, the case of Reunion island," *Renewable Sustain. Energy Rev.*, vol. 16, no. 1, pp. 426–442, 2012.
- [8] N. Duić and M. da Graça Carvalho, "Increasing renewable energy sources in island energy supply: Case study porto santo," *Renewable Sustain. Energy Rev.*, vol. 8, no. 4, pp. 383–399, 2004.
- [9] F. Chen, N. Duić, L. M. Alves, and M. da Graça Carvalho, "Renewable energy solutions for islands," *Renewable Sustain. Energy Rev.*, vol. 11, no. 8, pp. 1888–1902, 2007.
- [10] H. Haehne, J. Schottler, M. Waechter, J. Peinke, and O. Kamps, "The footprint of atmospheric turbulence in power grid frequency measurements," *EPL (Europhys. Lett.)*, vol. 121, no. 3, 2018, Art. no. 30001.
- [11] M. F. Wolff, K. Schmietendorf, P. G. Lind, O. Kamps, J. Peinke, and P. Maass, "Heterogeneities in electricity grids strongly enhance non-Gaussian features of frequency fluctuations under stochastic power input," *Chaos: An Interdiscipl. J. Nonlinear Sci.*, vol. 29, no. 10, 2019, Art. no. 103149.
- [12] P. Tielens and D. Van Hertem, "Grid inertia and frequency control in power systems with high penetration of renewables," in *Proc. Young Researchers Symp. Elect. Power Eng.*, 2012, pp. 1–6.

- [13] A. Ulbig, T. S. Borsche, and G. Andersson, "Impact of low rotational inertia on power system stability and operation," *IFAC Proc. Vol.*, vol. 47, no. 3, pp. 7290–7297, 2014.
- [14] M. Jabir, H. Azil Illias, S. Raza, and H. Mokhlis, "Intermittent smoothing approaches for wind power output: A review," *Energies*, vol. 10, no. 10, 2017, Art. no. 1572.
- [15] N. Hamsic et al., "Increasing renewable energy penetration in isolated grids using a flywheel energy storage system," in *Proc. IEEE Int. Conf. Power Eng., Energy Electric. Drives*, 2007, pp. 195–200.
- [16] G. Delille, B. Francois, and G. Malarange, "Dynamic frequency control support by energy storage to reduce the impact of wind and solar generation on isolated power system's inertia," *IEEE Trans. Sustain. Energy*, vol. 3, no. 4, pp. 931–939, Oct. 2012.
- [17] H. Zhao, Q. Wu, S. Hu, H. Xu, and C. N. Rasmussen, "Review of energy storage system for wind power integration support," *Appl. Energy*, vol. 137, pp. 545–553, 2015.
- [18] X. Li, D. Hui, and X. Lai, "Battery energy storage station (BESS)-based smoothing control of photovoltaic (PV) and wind power generation fluctuations," *IEEE Trans. Sustain. Energy*, vol. 4, no. 2, pp. 464–473, Apr. 2013.
- [19] F. Milano, F. Dörfler, G. Hug, D. J. Hill, and G. Verbič, "Foundations and challenges of low-inertia systems," in *Proc. Power Syst. Computation Conf.*, 2018, pp. 1–25.
- [20] B. Mohandes, M. S. El Moursi, N. Hatziaargyriou, and S. El Khatib, "A review of power system flexibility with high penetration of renewables," *IEEE Trans. Power Syst.*, vol. 34, no. 4, pp. 3140–3155, Jul. 2019.
- [21] X. Liang, "Emerging power quality challenges due to integration of renewable energy sources," *IEEE Trans. Ind. Appl.*, vol. 53, no. 2, pp. 855–866, Mar./Apr. 2016.
- [22] P. Denholm and M. Hand, "Grid flexibility and storage required to achieve very high penetration of variable renewable electricity," *Energy Policy*, vol. 39, no. 3, pp. 1817–1830, 2011.
- [23] P. Denholm and R. M. Margolis, "Evaluating the limits of solar photovoltaics (PV) in traditional electric power systems," *Energy Policy*, vol. 35, no. 5, pp. 2852–2861, 2007.
- [24] Anuario Energético Canarias, 2019. [Online]. Available: <http://www.gobiernodecanarias.org/istac/jaxi-istac/descarga.do?uripx=urn:uu id:03339289-7e10-49e9-a0a8-48db16496b89>
- [25] E. T. Tchuisseu, D. Gomila, D. Brunner, and P. Colet, "Effects of dynamic-demand-control appliances on the power grid frequency," *Phys. Rev. E*, vol. 96, no. 2, 2017, Art. no. 022302.
- [26] E. B. T. Tchuisseu, D. Gomila, P. Colet, D. Witthaut, M. Timme, and B. Schäfer, "Curing Braess' paradox by secondary control in power grids," *New J. Phys.*, vol. 20, no. 8, 2018, Art. no. 083005.
- [27] H. Saadat et al., *Power System Analysis*, vol. 2. New York, NY, USA: McGraw-Hill, 1999.
- [28] G. Filatrella, A. H. Nielsen, and N. F. Pedersen, "Analysis of a power grid using a Kuramoto-like model," *Eur. Phys. J. B*, vol. 61, no. 4, pp. 485–491, 2008.
- [29] T. Nishikawa and A. E. Motter, "Comparative analysis of existing models for power-grid synchronization," *New J. Phys.*, vol. 17, no. 1, 2015, Art. no. 015012.
- [30] M. Martínez-Barbeito and P. Colet, "Code repository," 2022. Online. Available: <https://gitlab.ifisc.uib-csic.es/power-grid/f90model/>
- [31] Q. Peng, Q. Jiang, Y. Yang, T. Liu, H. Wang, and F. Blaabjerg, "On the stability of power electronics-dominated systems: Challenges and potential solutions," *IEEE Trans. Ind. Appl.*, vol. 55, no. 6, pp. 7657–7670, Nov./Dec. 2019.
- [32] K. P. Nnoli, F. Delić, and S. Kettemann, "Transient dynamics and propagation of voltage and frequency fluctuations in transmission grids," 2022. [Online]. Available: <https://doi.org/10.36227/techrxiv.21298494.v1>
- [33] A. Sajadi, R. W. Kenyon, and B.-M. Hodge, "Synchronization in electric power networks with inherent heterogeneity up to 100% inverter-based renewable generation," *Nature Commun.*, vol. 13, no. 1, pp. 1–12, 2022.
- [34] M. H. Athari and Z. Wang, "Interdependence of transmission branch parameters on the voltage levels," in *Proc. 51st Hawaii Int. Conf. Syst. Sci.*, 2018, pp. 2757–2765.
- [35] Red Eléctrica de España, "Demanda de energía eléctrica en tiempo real," 2022. [Online]. Available: <https://demanda.ree.es/visiona/home>
- [36] Deloitte, "Los Territorios No Peninsulares 100% descarbonizados en 2040: la vanguardia de la transición energética en España," 2020. [Online]. Available: <https://www2.deloitte.com/es/es/pages/strategy/articles/territorios-no-peninsulares-descarbonizados-2040.html>
- [37] J. D. Glover, M. S. Sarma, and T. Overbye, *Power System Analysis & Design, SI Version*. Boston, MA, USA: Cengage Learning, 2012.
- [38] L. R. Gorjão et al., "Data-driven model of the power-grid frequency dynamics," *IEEE Access*, vol. 8, pp. 43082–43097, 2020.
- [39] R. Jumar, H. Maaß, B. Schäfer, L. R. Gorjão, and V. Hagenmeyer, "Database of power grid frequency measurements," 2020, *arXiv:2006.01771*.
- [40] L. Rydin Gorjão et al., "Open database analysis of scaling and spatio-temporal properties of power grid frequencies," *Nature Commun.*, vol. 11, no. 1, pp. 1–11, 2020.
- [41] M. for Ecological Transition, Boletín Oficial del Estado, 2019. [Online]. Available: [https://www.boe.es/eli/es/res/2019/12/11/\(3\)](https://www.boe.es/eli/es/res/2019/12/11/(3))
- [42] M. Anvari, L. R. Gorjão, M. Timme, D. Witthaut, B. Schäfer, and H. Kantz, "Stochastic properties of the frequency dynamics in real and synthetic power grids," *Phys. Rev. Res.*, vol. 2, no. 1, 2020, Art. no. 013339.
- [43] B. Schäfer, C. Beck, K. Aihara, D. Witthaut, and M. Timme, "Non-Gaussian power grid frequency fluctuations characterized by Lévy-stable laws and superstatistics," *Nature Energy*, vol. 3, no. 2, pp. 119–126, 2018.
- [44] M. Perez, R. Perez, K. R. Rábago, and M. Putnam, "Overbuilding & curtailment: The cost-effective enablers of firm PV generation," *Sol. Energy*, vol. 180, pp. 412–422, 2019.

María Martínez-Barbeito received the B.Sc. degree in physics from the Universidade de Santiago de Compostela (USC), Santiago, Spain, in 2018, and the M.Sc. degree in physics of complex systems in 2019 from the Universitat de les Illes Balears (UIB), Palma, Spain, where she is currently working toward the Ph.D. degree.

Damià Gomila received the M.Sc. degree in physics from the University of Barcelona, Barcelona, Spain, in 1998, and the Ph.D. degree from the Universitat de les Illes Balears, Palma, Spain, in 2003. He currently has a permanent research position with IFISC (CSIC-UIB), Institute for Cross-Disciplinary Physics and Complex Systems, Palma de Mallorca, Spain. His research interests include statistical and nonlinear physics and dynamical systems theory with applications to ecology and sociotechnical systems. Recent works focus on the effects of smart devices and renewable energy sources on the dynamics and stability of the power grid.

Pere Colet received the M.Sc. degree in physics from the Universitat de Barcelona, Barcelona, Spain, in 1987, and the Ph.D. degree from Universitat de les Illes Balears, Palma, Spain, in 1991. Since May 2007, he has been a Research Professor with the Spanish Consejo Superior de Investigaciones Científicas. He was a Postdoctoral Fulbright Fellow with the Georgia Institute of Technology, Atlanta, GA, USA. In May 1995, he joined CSIC. He has coauthored more than 140 articles. He has worked on fluctuations in nonlinear optical systems, switch-on time in lasers, synchronization of nonlinear oscillators, delay feedback effects, encoded communications based on chaotic lasers, coherence in laser arrays, pattern formation, quantum fluctuations in optical patterns, noise-sustained structures, front dynamics, localized structures, generation of high spectral purity microwaves with opto-electronic oscillators, and, more recently, the dynamics of the power grid and the analysis of human mobility using geolocated data.